letters to nature

Asian monsoon and the Indian Ocean dipole[25,26].

Models have been used to investigate the regional effect of varying the magnitude of the ITF on the Indian Ocean upper layer heat content and sea surface temperature[5–9]. Changes in the sea surface temperature associated with changes in the ITF transport shift the position of the deep atmosphere convection region of the western tropical Pacific[8,27] and, by changing the sea surface temperature in the Indian Ocean, alter the net evaporation within the Indian Ocean with consequences for the monsoon[7,8,28]. Although models investigate the contrast between 'off' and 'on' ITF[5–9], they do not explicitly consider the effects or causes of varying the ITF transport and temperature profiles, yet changes in their relationship, even without changes in the net transport, may be expected to alter the sea surface temperature and heat budget of the Pacific and Indian oceans and associated climate phenomena. □

1. Gordon, A. L. in *Ocean Circulation and Climate: Observing and Modeling the Global Ocean* (ed. Gould, J.) 303–314 (Academic, San Diego, 2001).
2. Gordon, A. L. & Fine, R. A. Pathways of water between the Pacific and Indian Oceans in the Indonesian seas. *Nature* **379,** 146–149 (1996).
3. Ffield, A., Vranes, K., Gordon, A. L., Susanto, R. D. & Garzoli, S. L. Temperature variability within Makassar Strait. *Geophys. Res. Lett.* **27,** 237–240 (2000).
4. Vranes, K., Gordon, A. L. & Ffield, A. The heat transport of the Indonesian Throughflow and implications for the Indian Ocean heat budget. *Deep-Sea Res. II* **49,** 1391–1410 (2002).
5. Lee, T., Fukumori, I., Menemenlis, D., Xing, Z. & Fu, L. Effects of the Indonesian Throughflow on the Pacific and Indian Oceans. *J. Phys. Oceanogr.* **32,** 1404–1429 (2002).
6. Hirst, A. C. & Godfrey, J. S. The role of Indonesian Throughflow in a global ocean GCM. *J. Phys. Oceanogr.* **23,** 1057–1086 (1993).
7. Godfrey, S. The effect of the Indonesian Throughflow on ocean circulation and heat exchange with the atmosphere: A review. *J. Geophys. Res.* **101,** 12217–12237 (1996).
8. Wajsowicz, R. Air-sea interaction over the Indian Ocean due to variations in the Indonesian Throughflow. *Clim. Dyn.* **18,** 437–453 (2002).
9. Wajsowicz, R. & Schneider, E. K. The Indonesian throughflow's effect on global climate determined from the COLA coupled climate system. *J. Clim.* **14,** 3029–3042 (2001).
10. Ilahude, A. G. & Gordon, A. L. Thermocline stratification within the Indonesian Seas. *J. Geophys. Res.* **101,** 12401–12409 (1996).
11. Van Aken, H. M., Punjanan, J. & Saimima, S. Physical aspects of the flushing of the east Indonesian basins. *Neth. J. Sea Res.* **22,** 315–339 (1988).
12. Piola, A. R. & Gordon, A. L. On oceanic heat and fresh-water fluxes at 30°S. *J. Phys. Oceanogr.* **16,** 2184–2190 (1986).
13. Toole, J. M. & Warren, B. A. A hydrographic section across the subtropical South Indian Ocean. *Deep-Sea Res. I* **40,** 1973–2019 (1993).
14. Robbins, P. E. & Toole, J. M. The dissolved silica budget as a constraint on the meridional overturning circulation of the Indian Ocean. *Deep-Sea Res. I* **44,** 879–906 (1997).
15. Macdonald, A. M. Property fluxes at 30S and their implications for the Pacific-Indian throughflow and the global heat budget. *J. Geophys. Res.* **98,** 6851–6868 (1993).
16. Ganachaud, A. & Wunsch, C. Improved estimates of global ocean circulation, heat transport and mixing from hydrographic data. *Nature* **408,** 453–457 (2000).
17. Ganachaud, A. & Wunsch, C. Large-scale ocean heat and freshwater transports during the World Ocean Circulation Experiment. *J. Clim.* **16,** 696–705 (2003).
18. Gordon, A. L., Susanto, R. D. & Ffield, A. Throughflow within Makassar Strait. *Geophys. Res. Lett.* **26,** 3325–3328 (1999).
19. Molcard, R., Fieux, M. & Ilahude, A. G. The Indo-Pacific throughflow in the Timor Passage. *J. Geophys. Res.* **101,** 12411–12420 (1996).
20. Molcard, R., Fieux, M. & Syamsudin, F. The throughflow within Ombai Strait. *Deep-Sea Res. I* **48,** 1237–1253 (2001).
21. Murray, S. P. & Arief, D. Throughflow into the Indian Ocean through the Lombok Strait, January 1985–January 1986. *Nature* **333,** 444–447 (1988).
22. Oberhuber, J. M. *An Atlas Based on "COADS" Data Set* (Tech. Rep. 15, Max-Planck-Institut für Meteorologie, Hamburg, 1988).
23. Wyrtki, K. *Physical Oceanography of the Southeast Asian Waters* (NAGA Rep. 2, Scripps Institution of Oceanography, La Jolla, 1961).
24. Mariano, A. J., Ryan, E. H., Perkins, B. D. & Smithers, S. *The Mariano Global Surface Velocity Analysis* 55 (United States Coast Guard, Washington DC, 1995).
25. Saji, N. H., Goswami, B. N., Vinayachandran, P. N. & Yamagata, T. A dipole mode on the tropical Indian Ocean. *Nature* **401,** 360–363 (1999).
26. Susanto, R. D., Gordon, A. L. & Zheng, Q. N. Upwelling along the coasts of Java and Sumatra and its relation to ENSO. *Geophys. Res. Lett.* **28,** 1599–1602 (2001).
27. Schneider, N. The Indonesian throughflow and the global climate system. *J. Clim.* **11,** 676–689 (1998).
28. Wajsowicz, R. C. & Schopf, P. S. Oceanic influences on the seasonal cycle in evaporation over the Indian Ocean. *J. Clim.* **14,** 1199–1226 (2001).
29. Conkright, M. E. *et al. World Ocean Atlas CD-ROM Data Set Documentation* (Internal Report 15, National Oceanographic Data Center, Silver Spring, Maryland, 1998).

Correspondence and requests for material should be addressed to A.L.G. (agordon@ldeo.columbia.edu).

Independent rate and temporal coding in hippocampal pyramidal cells

John Huxter[1]*, Neil Burgess[1,2] & John O'Keefe[1,2]

[1]*Department of Anatomy and Developmental Biology,* [2]*Institute of Cognitive Neuroscience, University College London, Gower Street, London WC1E 6BT, UK*

* Present address: Department of Anatomy, University of Bristol, Bristol BS8 1TD, UK

In the brain, hippocampal pyramidal cells use temporal[1] as well as rate[2] coding to signal spatial aspects of the animal's environment or behaviour. The temporal code takes the form of a phase relationship to the concurrent cycle of the hippocampal electroencephalogram theta rhythm[1]. These two codes could each represent a different variable[3,4]. However, this requires the rate and phase to vary independently, in contrast to recent suggestions[5,6] that they are tightly coupled, both reflecting the amplitude of the cell's input. Here we show that the time of firing and firing rate are dissociable, and can represent two independent variables: respectively the animal's location within the place field, and its speed of movement through the field. Independent encoding of location together with actions and stimuli occurring there may help to explain the dual roles of the hippocampus in spatial and episodic memory[7,8], or may indicate a more general role of the hippocampus in relational/declarative memory[9,10].

A cell must fire to manifest either a temporal or a rate code. Place cells are hippocampal pyramidal cells that increase their firing rate in a particular portion of the environment[2,11] (the 'place field', Fig. 1b). As such, they provide a coarse rate code for the animal's location within which a temporal code provides additional information[1,12,13]. In addition, we propose that the rate of firing within the field can vary to encode other information without disrupting this temporal code.

We recorded the firing of place cells and the electroencephalogram (EEG) from the hippocampi of rats as they ran back and forth on a linear track for food reward at each end (Fig. 1a, Methods). During this behaviour, the EEG shows the prominent theta oscillation and each place cell fires in a specific region of the track (Fig. 1b). The cell's bursting rate through the field (Fig. 1c) is slightly higher than the concurrent EEG theta frequency, so that the average phase of firing moves earlier on each theta wave as the animal progresses through the field (Fig. 1d). The phase of firing correlates with spatial variables such as the animal's position on the track or within the field (Fig. 1d), and also with non-spatial variables such as the time since entry into the field (Fig. 1e) or instantaneous firing rate (IFR; Fig. 1f), but in general the correlation with position is stronger than with either (Fig. 1g; see also refs 1, 5, 6, 12). Some process must align the phase of each spike relative to the concurrent theta wave so that the phase codes for location despite the different speeds of each run through the field.

Must the phase and rate codes always co-vary with each other, or

is it possible for them to dissociate? Harris et al.[5] reported an overall relationship between phase and rate in spikes recorded on a linear track, and our data show a similar relationship (Fig. 1g; Supplementary Fig. 1a, b). However, it is much weaker than the relationship between phase and position (Fig. 1d; phase correlates better with position than rate in 66/77 cells, $P = 5.3 \times 10^{-11}$), and may result directly from the relationship that both phase and rate hold with position (Supplementary Fig. 1c). Mehta and colleagues[6] reported that, over the first few runs of a session, the firing fields became more negatively skewed versus position and the phase precession strengthened—suggesting that both rate and phase reflect the net input to the cell and that this input becomes ramp-shaped, increasing with distance through the field. Our fields show a continuous range of negative, zero and positive skew, but there was no correlation between skew and the rate or amount of phase precession (Supplementary Fig. 2). Thus a causal relationship between negative field skew and phase precession is unlikely, despite both effects strengthening over the first few runs of a session.
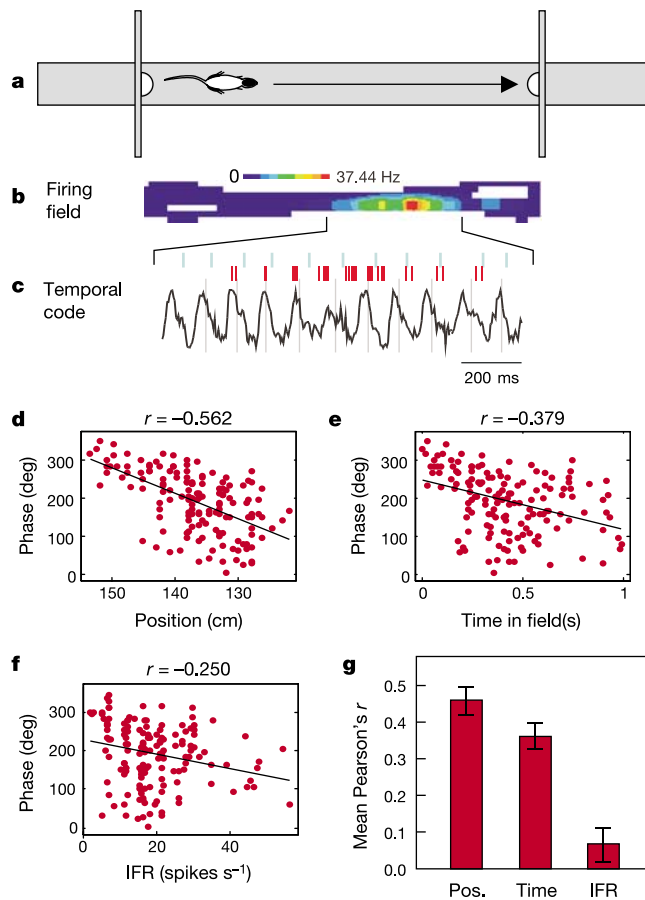
To see whether phase and rate dissociate within a place field, each field was divided into three equal segments: the beginning, middle and end. The mean IFR and mean firing phase per theta cycle, and their respective temporal derivatives (TD_{IFR} and TD_{phase}) for runs through each segment of the field were averaged across the population (Fig. 2). The mean phase per cycle continues to precess throughout the entire run, despite the firing rate rising in the early part of the field and then falling, and despite the increasing variance of firing phase through the field[6,14]. TD_{IFR} is positive in the early part of the field and negative in the late part, while TD_{phase} is negative throughout, demonstrating that phase precession occurs during both accelerating and decelerating spike trains, and that the firing rate rises and falls within each run. Thus, again, a causal relationship between phase precession and increasing rate is unlikely, consistent with the much lower correlation of phase with firing rate than with position (Fig. 1).

To see whether rate and phase dissociate on a run-by-run basis, the runs with the highest and lowest firing rates for each cell were identified so that the phase precession in both data sets could be compared. Across the population, we found no difference in mean phase precession between the high- and low-firing-rate runs. Figure 3 shows that phase precession takes place equally on trials with low as well as high firing rates, and even under conditions of very low firing rates with two or fewer spikes per run (Fig. 3b). Thus the dissociation of firing rate and firing phase is not due to effects specific to the second part of the field such as habituation, spike frequency accommodation, or to high- and low-rate runs being combined in the overall mean rate. In addition, the above data rule out any necessary coupling between phase precession and TD_{IFR} (compare ref. 5).

If the phase and firing rate can be independent, what variables

Figure 1 Place cell phase of firing correlates best with position. **a**, Behavioural task: rat shuttles back and forth along linear track between food rewards contained in cups attached to movable walls. **b**, False-colour firing field of a place cell created from multiple runs in the eastward direction. **c**, EEG theta rhythm and place cell firing (in red) for the same cell on a single eastward run. Ticks above the spikes indicate + to − zero crossings (0°/360° phase) for each theta wave, lines through theta waves indicate 270°. Bursts of spikes occur at higher than theta frequency causing each successive burst to move to an earlier phase of the theta cycle, despite initially rising, then falling firing rate. Theta cycle phase of spikes for multiple runs from a place cell is plotted against position (**d**), time (**e**) and instantaneous firing rate (IFR; **f**) in the place field. **g**, Phase (adjusted for circularity, see Methods) is better correlated with location than with time or firing rate across the population of cells. Here and in subsequent figures, vertical bars represent ±s.e.m.
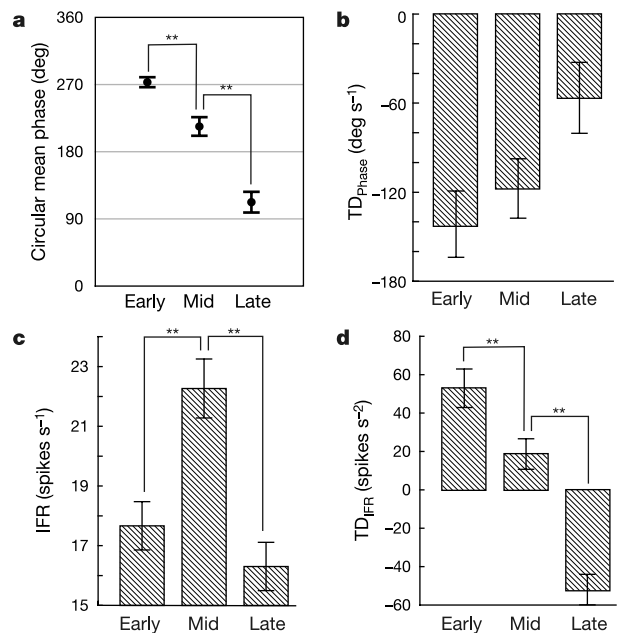

Figure 2 Phase precession is independent of IFR. **a**, Phase depends on location, being highest in the early third of each field, lower in the middle third, and lowest in the late third. **b**, Temporal derivative of phase (TD_{phase}) is negative in each portion of the field (68/76 fields in the early portion, $P < 1 \times 10^{-12}$; 57/76 in the middle, $P < 1 \times 10^{-5}$; 46/76 late, $P < 0.05$, binomial test). **c**, IFR starts low, increases in the middle third and then decreases in the late part of the field. **d**, Temporal derivative of instantaneous firing rate (TD_{IFR}) starts high, falls towards zero in the middle third, and then goes negative in the last third. Here and in subsequent figures, an asterisk denotes $P < 0.05$, and a double asterisk denotes $P < 0.01$.
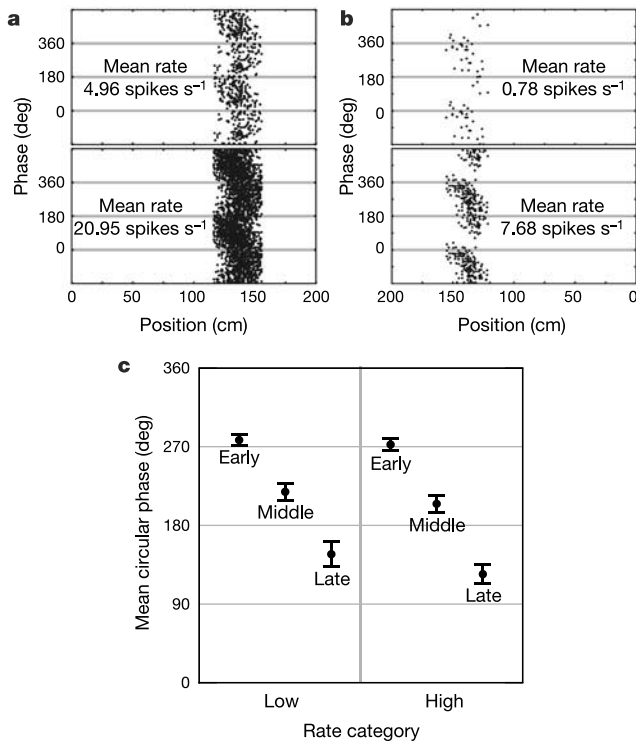
Figure 4 Firing rates differ on fast and slow runs through the field. **a**, Significant difference in average peak firing rates but no difference in **b**, rate of phase precession, or **c**, total phase shift. **d**, Firing rate is the only variable measured that consistently correlates with running speed (1.5 m track, mean $r = 0.223$, 23/29 fields with significant positive correlations $P < 0.05$).

Figure 3 Phase is correlated with track location on low- as well as high-firing-rate runs. **a**, A single cell for which average firing rate on high-rate runs (lower panel) is four times that on lower rate ones (upper panel) with no discernible effect on the phase precession. **b**, The same analysis for the cell shown in Fig. 1d–f. Phase precession occurs despite very low firing rates. Above: 35 spikes from 66 low-rate runs, mean spikes per run 0.53, s.e.m. 0.09, range 0–2 (0 spikes on 41 runs, 1 on 15, and 2 on 10); below: 194 spikes from 36 high-rate runs, mean spikes per run 5.40, s.e.m. 0.53, range 2–14. **c**, Population data ($n = 34$): phase precesses across early, middle and late parts of the field on both high- and low-rate runs.

does each encode? Previous work has suggested that the firing rate of place cells correlates with running speed through the field[15–18]. We confirm that relationship for the present data set (Fig. 4), where place fields reconstructed from faster runs were associated with higher firing rates (30 of 34 fields, $t_{1,33} = -5.88, P < 0.001$; Fig. 4a). In contrast, the temporal code did not vary between fast and slow runs, as measured by mean rate of phase precession in space ($t_{1,33} = 0.301, P = 0.77$; Fig. 4b); total extent of phase precession ($t_{1,33} = -4.32, P = 0.67$; Fig. 4c); phase at firing onset ($F_{1,32} = 0.066, P = 0.799$) or offset ($F_{1,32} = 1.281, P = 0.266$; data not shown). The correlation between mean firing rate per run and running speed on individual runs, averaged across the population, is 0.223 (Fig. 4d)—higher than the correlation between speed and any other variable that we have measured.

To identify the spatial correlate of firing phase more precisely, we varied the length of the track from 1.5 m to 1.0 m or 0.75 m by moving the end walls closer together. The rats ran slower on the shortened tracks ($F_{1,29} = 12.536, P = 0.001$), the fields were smaller ($F_{1,29} = 16.834, P < 0.001$) and firing rates were reduced ($F_{1,29} = 11.068, P = 0.002$) (Fig. 5a). When the fields shrank, there was a strong correlation between the shortening of a field and the increase in the rate of change of phase in space (Fig. 5b). By contrast, the change in the rate of phase precession was not correlated with changes in its firing rate (Fig. 5c). We tentatively conclude that the phase is coding for the proportion of the field traversed, which is also consistent with the finding that blocking long-term potentiation (LTP) produces shorter fields on average (by
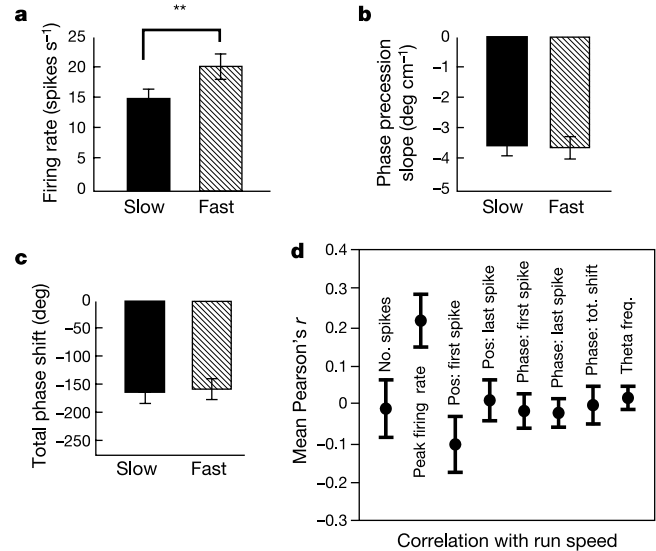
preventing their asymmetric expansion[19]) but does not reduce the amount of phase precession[18]. The correlation between running speed and firing rate per run observed on the full-length track was also found on the shortened track (mean $r = 0.18$), showing the robustness of this effect within different environmental configurations.

What mechanisms might underlie phase coding of location independent of rate? One model[1,20] views CA3 place-cell firing as an interference pattern between an inhibitory theta input and an intrinsically oscillatory membrane potential (see, for example, ref. 21), whose frequency increases above theta frequency as the input to the cell increases (see, for example, ref. 22). Under this model, modulation of the amplitudes of the response, possibly by input from the dentate gyrus, need not affect its phase, while the rate of precession naturally adjusts to cover the extent of the field. If the frequency of the variable oscillator reflects distance from landmarks as measured by external and internal signals including motor efference, this model could also account for the phase precession observed in running wheels as well as linear tracks[5]. Alternative possibilities include phase of firing reflecting the directions of the stimuli defining the place field[3,23], or early-field firing being driven by input from other place cells while late-field firing is driven by sensory input[19,24–26]. In this latter model, delays in synaptic transmission mean that early-field firing occurs later in a theta cycle than that driven by sensory input (note, however, that the drive from other place cells should not depend on LTP[18]).

The present experiments show that, on linear tracks, the phase of firing relative to the hippocampal EEG theta wave and the IFR code for two independent aspects of the animal's spatial behaviour: proportion of distance through the place field, and in-field velocity. But the correlation of rate with velocity varies between cells and is low overall, suggesting that it might also code for other variables. Previous experiments[2,16,27,28] suggest that firing rate in the place field is influenced by such variables as direction of turning along the rat's trajectory and the presence (or absence) of particular objects, or of smells or sounds associated with reinforcers. Thus we propose that the strong spatial relation with phase leaves modulation of the firing rate free to represent additional information regarding the beha-
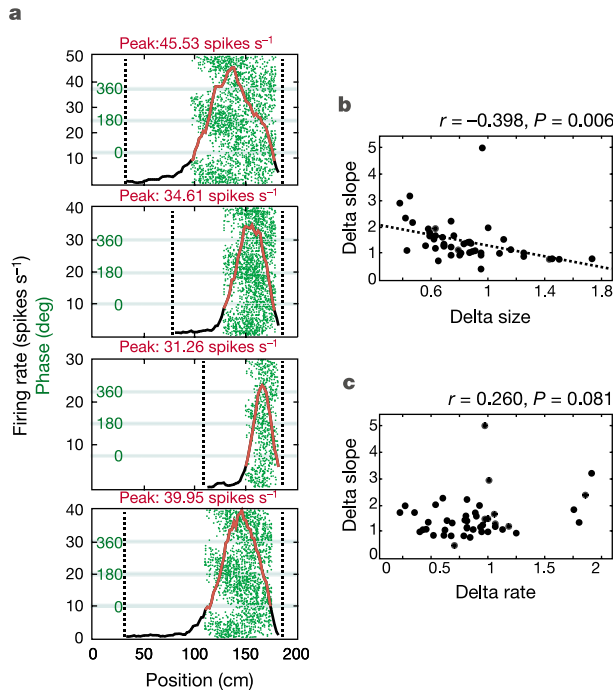
Figure 5 Phase precession on the shortened tracks. Single cell: **a**, phase angle versus position (green) gets steeper as the field size shrinks and the field firing rate (spikes dividing by dwell time, in red) drops owing to shortening of the track. Bottom panel shows the second baseline trial on full-length track carried out after short track trials. Population: slope of phase precession (that is rate of change in space) increases with shorter track length (**b**) in the absence of systematic changes in other correlations such as firing rate (**c**). 'Delta' values refer to the change from the preceding baseline trial to the trial on the shortened track (see Methods).

viours performed and the salient objects or features encountered in specific places. This dual code may provide the neural basis for the involvement of the hippocampus in both spatial and more general episodic/declarative memory[7–10] by simultaneously encoding and binding together the location of the event and its behavioural and sensory content. Theta EEG activity has also been demonstrated in many different neocortical regions in human patients[29], suggesting that the ability to code for more than one variable by using rate and temporal codes may be a general property of cortical pyramidal cells. □

Methods

Experimental procedure

Nine male Lister hooded rats were implanted with pairs of movable tetrodes in the dorsal hippocampus[1,30], and placed on a food deprivation schedule (initially reduced to 90% of body weight with a subsequent gain of 5 g week^{-1}). After one week of post-operative recovery, they were trained to shuttle between the ends of a linear track for food reward (track dimensions: 150 × 10 cm, bounded by 25 cm side walls and 61 cm end walls that could be moved to shorten the length of the track). Above the walls, the rats could see the experimental room. A recording session consisted of a series of 8-min trials, the first always a set of runs on the full-length track followed by a series of trials including trials on shortened tracks, interspersed with baseline full-length track trials. Further series were then run in which the size of the end walls was modified or the belt which comprised the floor of the track was moved. Only the results from the first series are reported here.

An overhead camera tracked an array of infrared light-emitting diodes (LEDs) fixed to the rat's head (sampled at 50 Hz with a theoretical resolution of 3 mm). Simultaneously, EEG field potentials (sampled at 250 Hz, band-pass filtered at 0.34–125 Hz) and extracellular action potentials (spikes, sampled at 48 kHz, band-pass filtered at 500–6,700 Hz) were recorded from the pyramidal cell layer. Half-sinusoids in the theta frequency range (6–16 Hz) were aligned to negative-going deflections in the EEG and the goodness-of-fit used to detect the presence of theta. The firing phase (0–359°) of a spike reflects its temporal distance between successive zero crossings during theta. Where absolute phase values from different fields are combined, each field is first adjusted by a constant so that least frequent phase corresponds to 0°/360°.

Place field definition

For a given cell, firing rates were calculated in 2 cm bins along the length of the track (that is, the ratio of the total number of spikes to occupancy duration in each bin) and then boxcar-averaged using the five bins centred on it. Place fields were defined as the bin with the highest firing rate and all contiguous bins in which the firing rate exceeded 20% of this peak rate.

General data analysis

Only well-isolated units with good spatial selectivity and a peak firing rate of >1 Hz were analysed, yielding 73 cells with 94 place fields: 75 from CA1, 19 from CA3, the dentate gyrus or hilar region. All further analyses concerned data from runs through the place field in its preferred firing direction at above 10 cm s^{-1}. Positions are plotted such that the ordinate increases for runs from east to west and decreases for runs from west to east. The initial trial on the full-length track from each place field was used to compare field characteristics such as peak firing rate, field skew, and rate of phase precession versus position. Correlations and regressions on phase data were adjusted to take account of its circular nature, minimizing the squared angular distance from the line rather than the squared absolute distance (see also ref. 1). Correlations were done on the 77 fields contributing at least 100 spikes to the initial full-length trial.

IFR was calculated as the number of spikes in a time window up to one theta cycle on either side of the reference spike, divided by the size of the window (after ref. 5). The temporal derivative of the IFR (TD$_{IFR}$) is the difference between the IFR for any two consecutive spikes, divided by the time interval between them. Only IFRs based on time windows greater than 100 ms were included. Mean phase per cycle is the circular mean phase of spikes within a theta cycle, and the temporal derivative of this (TD$_{phase}$) is the circular difference between the mean phase in successive theta cycles divided by the duration of the first cycle.

For analyses comparing fast versus slow runs and high-rate versus low-rate runs (Figs 3c and 4a–c), separate fields were constructed from subsets of runs (combining multiple baseline trials with $r > 0.9$ field correlations). 'Slow runs' comprised those containing the bottom quartile of spikes ordered by the speed of the run through the firing field (that is, the length of the path through the field divided by its duration), 'fast runs' comprised the top quartile. Four fields for which this produced fewer than 200 spikes in each subset were simply split at the 50th percentile. Runs ordered by firing rate were divided into 'high' and 'low' rate runs at the 50th percentile of the firing rate. In both cases, only fields for which there were at least 100 runs through the composite field were included ($n = 34$).

Shortened runway

Field characteristics on two shortened-runway trials (created by moving one of the end walls 50 or 75 cm towards the middle of the track) were compared with the two flanking baseline trials and analysed using a repeated measures analysis of variance. The wall that was moved and the amount by which it was moved varied pseudo-randomly across trials. Changes in firing rate, running speed, and field size were measured as the ratio of the score on each manipulation trial compared to the preceding baseline. Changes in the rate of precession were measured as the difference between scores on manipulation trials and the preceding baseline, and were only performed on trials with 100 or more spikes.

1. O'Keefe, J. & Recce, M. L. Phase relationship between hippocampal place units and the EEG theta rhythm. *Hippocampus* **3,** 317–330 (1993).
2. O'Keefe, J. Place units in the hippocampus of the freely moving rat. *Exp. Neurol.* **51,** 78–109 (1976).
3. O'Keefe, J. in *Brain and Space* (ed. Paillard, J.) 273–295 (Oxford Univ. Press, Oxford, 1991).
4. Buzsaki, G. Theta oscillations in the hippocampus. *Neuron* **33,** 325–340 (2002).
5. Harris, K. D. *et al.* Spike train dynamics predicts theta-related phase precession in hippocampal pyramidal cells. *Nature* **417,** 738–741 (2002).
6. Mehta, M. R., Lee, A. K. & Wilson, M. A. Role of experience and oscillations in transforming a rate code into a temporal code. *Nature* **417,** 741–746 (2002).
7. O'Keefe, J. & Nadel, L. *The Hippocampus as a Cognitive Map* (Oxford Univ. Press, Oxford, 1978); ⟨www.cognitivemap.net⟩ (2003).
8. Burgess, N., Maguire, E. A. & O'Keefe, J. The human hippocampus and spatial and episodic memory. *Neuron* **35,** 625–641 (2002).
9. Squire, L. R. Memory and the hippocampus: A synthesis from findings with rats, monkeys, and humans. *Psychol. Rev.* **99,** 195–231 (1992).
10. Eichenbaum, H. & Cohen, N. *From Conditioning to Conscious Recollection* (Oxford Univ. Press, Oxford, 2001).
11. Muller, R. A quarter of a century of place cells. *Neuron* **17,** 813–822 (1996).
12. Skaggs, W. E., McNaughton, B. L., Wilson, M. A. & Barnes, C. A. Theta phase precession in hippocampal neuronal populations and the compression of temporal sequences. *Hippocampus* **6,** 149–172 (1996).
13. Jensen, O. & Lisman, J. E. Position reconstruction from an ensemble of hippocampal place cells: Contribution of theta phase coding. *J. Neurophysiol.* **83,** 2602–2609 (2000).
14. Yamaguchi, Y., Aota, Y., McNaughton, B. L. & Lipa, P. Bimodality of theta phase precession in hippocampal place cells in freely running rats. *J. Neurophysiol.* **87,** 2629–2642 (2002).
15. McNaughton, B. L., Barnes, C. A. & O'Keefe, J. The contributions of position, direction, and velocity to single unit activity in the hippocampus of freely-moving rats. *Exp. Brain Res.* **52,** 41–49 (1983).
16. Wiener, S. I., Paul, C. A. & Eichenbaum, H. Spatial and behavioral correlates of hippocampal neuronal activity. *J. Neurosci.* **9,** 2737–2763 (1989).
17. Hirase, H., Czurko, H. H., Csicsvari, J. & Buzsaki, G. Firing rate and theta-phase coding by hippocampal pyramidal neurons during 'space clamping'. *Eur. J. Neurosci.* **11,** 4373–4380 (1999).
18. Ekstrom, A. D., Meltzer, J., McNaughton, B. L. & Barnes, C. A. NMDA receptor antagonism blocks experience-dependent expansion of hippocampal "place fields". *Neuron* **31,** 631–638 (2001).
19. Mehta, M. R., Barnes, C. A. & McNaughton, B. L. Experience-dependent, asymmetric expansion of hippocampal place fields. *Proc. Natl Acad. Sci. USA* **94,** 8918–8921 (1997).

20. Lengyel, M., Szatmary, Z. & Erdi, P. Dynamically detuned oscillators account for the coupled rate and temporal code of place cell firing. *Hippocampus* **13**, 700–714 (2003).

21. Pike, F. G. *et al.* Distinct frequency preferences of different types of rat hippocampal neurones in response to oscillatory input currents. *J. Physiol. Lond.* **529**, 205–213 (2000).

22. Kamondi, A., Acsady, L., Wang, X. J. & Buzsaki, G. Theta oscillations in somata and dendrites of hippocampal pyramidal cells *in vivo*: Activity-dependent phase-precession of action potentials. *Hippocampus* **8**, 244–261 (1998).

23. Burgess, N., Recce, M. & O'Keefe, J. A model of hippocampal function. *Neural Netw.* **7**, 1065–1081 (1994).

24. Tsodyks, M. V., Skaggs, W. E., Sejnowski, T. J. & McNaughton, B. L. Population dynamics and theta rhythm phase precession of hippocampal place cell firing: A spiking neuron model. *Hippocampus* **6**, 271–280 (1996).

25. Jensen, O. & Lisman, J. E. Hippocampal CA3 region predicts memory sequences: Accounting for the phase precession of place cells. *Learn. Mem.* **3**, 279–287 (1996).

26. Wallenstein, G. V. & Hasselmo, M. E. GABAergic modulation of hippocampal population activity: Sequence learning, place field development, and the phase precession effect. *J. Neurophysiol.* **78**, 393–408 (1997).

27. Wood, E. R., Dudchenko, P. A. & Eichenbaum, H. The global record of memory in hippocampal neuronal activity. *Nature* **397**, 613–616 (1999).

28. Moita, M. A., Rosis, S., Zhou, Y., LeDoux, J. E. & Blair, H. T. Hippocampal place cells acquire location-specific responses to the conditioned stimulus during auditory fear conditioning. *Neuron* **37**, 485–497 (2003).

29. Kahana, M. J., Sekuler, R., Caplan, J. B., Kirschen, M. & Madsen, J. R. Human theta oscillations exhibit task dependence during virtual maze navigation. *Nature* **399**, 781–784 (1999).

30. O'Keefe, J. & Burgess, N. Geometric determinants of the place fields of hippocampal neurons. *Nature* **381**, 425–428 (1996).

....

A regulatory mutation in *IGF2* causes a major QTL effect on muscle growth in the pig

Anne-Sophie Van Laere[1]*, **Minh Nguyen**[3]*, **Martin Braunschweig**[1], **Carine Nezer**[3], **Catherine Collette**[3], **Laurence Moreau**[3], **Alan L. Archibald**[4], **Chris S. Haley**[4], **Nadine Buys**[5], **Michael Tally**[6], **Göran Andersson**[1], **Michel Georges**[3] & **Leif Andersson**[1,2]

[1]*Department of Animal Breeding and Genetics, Swedish University of Agricultural Sciences, and* [2]*Department of Medical Biochemistry and Microbiology, Uppsala University, BMC, Box 597, SE-751 24 Uppsala, Sweden*
[3]*Department of Genetics, Faculty of Veterinary Medicine, University of Liege (B43), 20, bd. de Colonster, 4000 Liege, Belgium*
[4]*Roslin Institute (Edinburgh), Roslin, Midlothian EH25 9PS, Scotland, UK*
[5]*Gentec, Kapelbaan 15, 9255 Buggenhout, Belgium*
[6]*Tally Consulting, SE-11458 Stockholm, Sweden*

* These authors contributed equally to this work

....

Most traits and disorders have a multifactorial background indicating that they are controlled by environmental factors as well as an unknown number of quantitative trait loci (QTLs)[1,2]. The identification of mutations underlying QTLs is a challenge because each locus explains only a fraction of the phenotypic variation[3,4]. A paternally expressed QTL affecting muscle growth, fat deposition and size of the heart in pigs maps to the *IGF2* (insulin-like growth factor 2) region[5,6]. Here we show that this QTL is caused by a nucleotide substitution in intron 3 of *IGF2*. The mutation occurs in an evolutionarily conserved CpG island that is hypomethylated in skeletal muscle. The mutation

abrogates *in vitro* interaction with a nuclear factor, probably a repressor, and pigs inheriting the mutation from their sire have a threefold increase in *IGF2* messenger RNA expression in post-natal muscle. Our study establishes a causal relationship between a single-base-pair substitution in a non-coding region and a QTL effect. The result supports the long-held view that regulatory mutations are important for controlling phenotypic variation[7].

The QTL affecting muscle growth, fat deposition and heart size was first identified in intercrosses between the European wild boar and Large White domestic pigs and between Piétrain and Large White pigs[5,6]. The alleles from the Large White breed in the first cross and the Piétrain breed in the second cross increased muscle mass and reduced back-fat thickness. The QTL explained 15–30% of the phenotypic variation in muscle mass and 10–20% of the variation in back-fat thickness[5,6]. We recently used a haplotype-sharing approach to refine the map position of the QTL[8]. We assumed that a new allele (Q) promoting muscle development occurred g generations ago on a chromosome carrying the wild-type allele (q). We also assumed that the favourable allele had gone through a selective sweep due to the strong selection for lean growth in commercial pig populations. A QTL genotype cannot be deduced directly from an individual's phenotype but the QTL genotype of sires can be determined by progeny testing and marker-assisted segregation analysis[2]. Twenty-eight chromosomes with known QTL status were identified. All 19 Q-bearing chromosomes shared a haplotype in the 250-kilobase (kb) interval between the markers *370SNP6/15* and *SWC9* (*IGF2* 3′ untranslated region), which was therefore predicted to contain the QTL. This region contains *INS* and *IGF2* as the only known paternally expressed genes. Given their known functions and especially the role of *IGF2* in myogenesis[9], they stood out as prime positional candidates.

We re-sequenced one of the 19 Q chromosomes (P208) and six q chromosomes (each corresponding to a distinct marker haplotype) for a 28.6-kb segment containing *IGF2*, *INS* and the 3′ end of *TH*. This chromosome collection was expanded by including Q and q chromosomes from the following: (1) a wild boar/Large White intercross segregating for the QTL[5]; (2) a Swedish Landrace boar showing no evidence for QTL segregation in a previous study[10]; and (3) F$_1$ sires from a Hampshire/Landrace cross and a Meishan/Large White intercross both showing no indication for QTL segregation (see Methods). The lack of evidence for QTL segregation shows that the boars are either homozygous Q/Q or q/q. A Japanese wild boar was included as a reference for the phylogenetic analysis and it was assumed to be homozygous wild type (q/q). We identified a total of 258 DNA sequence polymorphisms corresponding to one polymorphic nucleotide per 111 base pairs (bp) (Fig. 1). Two major and quite divergent clusters of haplotypes were revealed (Supplementary Fig. 1). The two established Q haplotypes from Piétrain and Large White animals (P208 and LW3) were identical to each other and to the chromosomes from the Landrace (LRJ) and Hampshire/Landrace (H205) animals, showing that the latter two must be of Q type as well. The absence of QTL segregation in the offspring of the F$_1$ Hampshire × Landrace boar carrying the H205 and H254 chromosomes implies that the latter recombinant chromosome is also of Q type. This places the causative mutation downstream from *IGF2* intron 1, in the region for which H254 is identical to the other Q chromosomes. The Large White chromosome (LW197) from the Meishan/Large White pedigree clearly clustered with q chromosomes, implying that the F$_1$ sire used for sequencing was homozygous q/q as no overall evidence for QTL segregation was observed in this intercross. This is consistent with a previous study showing that Meishan pigs carry an *IGF2* allele associated with low muscle mass[11]. Surprisingly, the Meishan allele (M220) was nearly identical to the Q chromosomes but with one notable exception, it shared guanine with all q chromosomes at a position (*IGF2*-intron3-nucleotide 3072) where all Q chromosomes have adenine (Fig. 1).

Under a bi-allelic QTL model, the causative mutation would